



ARTICLE

Detection of Frost-Resistance Property of Large-Size Concrete Based on Impact-Echo Method

Qi Feng¹, Zhengyue Ren² and Dan Wang^{3,*}

¹Guangxi Transportation Science and Technology Group Co., Ltd., Nanning, 530007, China

²School of Civil Engineering, Dalian University of Technology, Dalian, 116024, China

³Special Glass Key Lab of Hainan Province & State Key Laboratory of Marine Resource Utilization in South China Sea, Hainan University, Haikou, 570228, China

*Corresponding Author: Dan Wang. Email: wangd_dlut@163.com

Received: 13 June 2022 Accepted: 23 August 2022

ABSTRACT

The dynamic elasticity modulus (E_d) is the most commonly used indexes for nondestructive testing to represent the internal damage of hydraulic concrete. Samples with a specific size is required when the transverse resonance method was used to detect the E_d , resulting in a limitation for field tests. The impact-echo method can make up defects of traditional detection methods for frost-resistance testing, such as the evaluation via the loss of mass or strength. The feasibility of the impact-echo method to obtain the relative E_d is explored to detect the frost-resistance property of large-volume hydraulic concretes on site. Results show that the impact-echo method can replace the traditional resonance frequency method to evaluate the frost resistance of concrete, and has advantages of high accuracy, easy to operate, and not affecting by the aggregate size and size effect of samples. The dynamic elastic modulus of concrete detected by the impact-echo method has little difference with that obtained by the traditional resonance method. The one-dimensional elastic wave velocity of concrete has a good linear correlation with the transverse resonance frequency. The freeze-thaw damage occurred from the surface to the inner layer, and the surface is expected to be the most vulnerable part for the freeze-thaw damage. It is expected to monitor and track the degradation of the frost resistance of an actual structure by frequently detecting the P-wave velocity on site, which avoids coring again.

KEYWORDS

Impact-echo method; frost-resistance property; dynamic elastic modulus; E_d ; elastic wave velocity; transverse resonance frequency

1 Introduction

The reasons for the destruction of concrete are (in descending order of significance): steel-bar corrosion, freeze-thaw damage, and other physical and chemical erosions induced by surrounding environment, which is reported by Mehta in the second international conference on concrete durability [1]. The mostly common evaluation parameters for frost-resistance at present are the mass loss, strength degradation, relative dynamic elasticity modulus. Besides, other parameters such as the fracture energy, strain [2], electrical resistivity [3], and water-saturation degree are also used to evaluate the freeze-thaw damage of concrete. Arnfelt [4] pointed



out, for the first time, that the freeze-thaw damage of concrete is expected to cause spall damage on the surface of concrete, so the mass loss is regarded as an indicator to estimate the frost-resistance of concrete [5]. Many scholars [6] hold that the degradation degree of compressive strength can reflect the degradation process during freezing and thawing cycles of concrete. So, the loss of compressive strength is also regarded as an important index to estimate the frost-resistance in the case of slow-freezing method.

However, both the mass loss and the strength loss have limitations. The mass loss only reflects the spall damage on the surface of concrete, and cannot represent the internal damage of concrete. Besides, previous research confirmed that the internal crack of high-strength concrete (such as C60 concrete) showed a rapid expand after 270–330 cycles of freeze-thaw tests, but almost no surface damage can be found during tests [7], which illustrates that the mass loss is not suitable to evaluate the frost-resistance of high-strength concrete. The strength loss is influenced by the molding quality. Especially, both of the indicators are only suitable to estimate the damage of concrete under laboratory conditions of freezing and thawing cycles, and not suitable for field tests regarding the hydraulic structure such as the port structure. The freeze-thaw cycle test in laboratory cannot simulate the real situation very well. It should be notice that the dynamic elasticity modulus (E_d) is the most commonly used indexes for nondestructive testing to represent the internal damage of hydraulic concrete.

The dynamic elasticity modulus depends on the inherent nature of the material itself, and changes with the internal structure of concrete. The dynamic elasticity modulus can reflect the whole and local damage of structure. At present, the transverse resonance method has been widely used to determine the dynamic elasticity modulus, and has been incorporated into standards in many countries, such as the earliest U.S. standard ASTM C666, the subsequent Japanese standard JIST1148, Canadian standard CSA-A23.2, Chinese standard GBJ82-85, and GB/T50082-2009. This method is based on the natural vibration frequency of concrete changed during the freeze-thaw cycle [8], and is only suitable for the control of the concrete quality under laboratory conditions. A laboratory freeze-thaw condition and core samples are needed when using the transverse resonance method, but it cannot completely replace the actual engineering conditions. A specific size of samples (usually a rod-like shape with a size of 100 mm × 100 mm × 400 mm) is required when the transverse resonance method was used, resulting in a limitation for field tests. The frequency of the stress wave generated by the impact-echo method during the instantaneous shock is low (~70 kHz), and it is not easy to be attenuated during the propagation of non-uniform media such as concrete [9]. The impact-echo method is more practical in determining the defect on concrete but has not been widely used to estimate the frost-resistance of concrete until now, especially for the large-size concrete.

The impact-echo method is a kind of nondestructive technologies and based on the transient stress wave. The testing procedure and calculation method for using impact-echo method in determining the wave velocity and resonance frequency can be found in standard ASTM C1383 [10] and ASTM C125 [11]. Using of the impact-echo technique to determine defects for concrete has been widely investigated, except for determining the frost-resistance of concrete. For example, impact-echo technique combined with electrochemistry method was used to accurately detect the development of micro-cracks in concrete blocks by Liang et al. [12], which proved that the impact-echo technique can be used to evaluate the corrosion damage in reinforced concrete structures. Impact-echo technique was used to test the degree of thermal damage of concrete by Krzemień et al. [13], and found that it showed a strong correlation between the obtained characteristic signal of impact-echo tests and the high temperature mechanical properties of concrete. The effect of the sensitivity of two methods including impact-echo technique and ultrasonic surface wave on different parameters in the concrete slab was investigated by Azari et al. [14], and found that their showed a high sensitivity for many parameters. The detection of size and thickness of concrete slabs are more sensitive as for the impact-echo technique. The impact-echo technique was used to evaluate the internal defects of concrete reported by Chaudhary [15], confirming that the results

obtained by this method are crucial basis for taking an appropriate repair plan. The impact-echo technique was used to evaluate the local bond loss of steel bars, and a method using non-destructive testing was established to determine the damaged of bond properties of steel bars in concrete structures destroyed by earthquakes [16]. The impact-echo method is easy to operate, and especially suitable for the defect evaluation of large-volume concrete. Zima [17] used the elastic wave to effectively monitor debonding damage parameters of reinforced concrete. Wandowski et al. [18] verified that the impact-echo method has a high accuracy in detecting voids and peeling defects through a combination of numerical calculation and experiment. Jagnathan [19] verified the accuracy of impact-echo method in detecting the compactness of concrete by using the method of pre-embedded defects. The dynamic elasticity modulus of concrete can be calculated from the wave velocity, and thus the frost-resistance of concrete can be evaluated via the impact-echo method.

The impact-echo method has several advantages; For example: 1) it can be used for field tests without specific requirements on sizes of samples, which makes up defects of traditional detection methods for frost-resistance testing; 2) it is a nondestructive technology with high precision in detecting the durability of structure [20,21]. The impact-echo signals are disturbed by the inner structure of concrete such as the porosity and moisture content, and are also disturbed by the design of measure points and the size of samples [22]. Therefore, the impact-echo method was carried out for different size of samples to verify whether it can be used to evaluate the frost-resistance property of large-size concrete in this study.

In this study, the evaluation of frost-resistance for physical construction using nondestructive technology (i.e., the impact-echo method) is explored to detect the state of hydraulic structure by field tests. The freeze-thaw tests on samples with different section size ranging from 100 to 500 mm were carried out to investigate the size effect on the impact-echo method. Researches on further expansion techniques of the impact-echo method in various application areas is beneficial for a better detecting the state of physical construction.

2 Experimental Programs

2.1 Material Design

The mix proportions were chosen according to the standard Test Code for Hydraulic Concrete (SL352-2020) [23], as shown in Table 1. The Portland cement of P•O42.5R (a kind of the Portland cement, which the 28 d compressive strength is higher than 42.5 MPa and has a higher strength at the early hydration stage) was provided by Dalian Onoda Cement Co., Ltd. (China).

Table 1: Mix proportions and physical properties of concrete

No.	w/c	Sand ratio (%)	Mix proportion (kg/m ³)				$f_{cu,28}$ (MPa)	Slump (mm)	Apparent density, ρ (kg/m ³)	Maximum particle size of coarse aggregate (mm)
			Water	Cement	Coarse aggregate	Sand				
L1	0.48	35	214.0	446.0	1102.0	593.0	47.55	82	2411.67	25
L2	0.55	43	215.0	391.0	1022.0	772.0	41.67	84	2390.83	25
S1	0.48	38	220.0	458.3	1067.5	654.2	47.00	75	2381.67	16
S2	0.55	43	220.0	400.0	1014.6	765.4	39.75	80	2382.50	16

2.2 Sample Preparation

Four groups of samples (named L1, L2, S1, S2) with a size of 100 mm × 100 mm × 400 mm were prepared according to the mix proportions listed in Table 1, so as to verify the consistency of results between the transverse resonance method and the impact-echo method in detecting the frost resistance. The size of 100 mm × 100 mm × 400 mm is chosen because it is a common size of samples for

conducting the transverse resonance method. The four groups of samples were cured for 7 and 28 d under standard conditions (95% RH, $20^{\circ}\text{C} \pm 2^{\circ}\text{C}$) prior to detect the velocity of elastic waves (P-wave, V_{p1} , m/s) and transverse frequency (f , Hz). The P-wave velocity can be calculated from the Eq. (1): where f represents the transverse frequency (Hz), L represents the specimen length (m).

$$V_{p1} = 2L \cdot f \quad (1)$$

Three specimens per group were measured. The dynamic modulus is calculated from the Eq. (2) when using the transverse resonance method. The dynamic modulus is calculated from the Eq. (3) when using the impact-echo method.

$$E_d = \frac{0.9464L^3k}{ab^3}mf^2 \quad (2)$$

where f represents the fundamental transverse frequency (Hz); m is the weight of a sample (kg); b and a are section sizes of a prism (m) with b being the size in the direction in which the sample is driven; k is a compensation coefficient, which is up to the ratio of gyration radius to the length of samples.

The theoretical propagation equations of P-wave in elastic media is shown as follows:

One-dimensional propagation:

$$V_{p1} = \sqrt{\frac{E_d}{\rho}} \quad (3)$$

Three-dimensional propagation:

$$V_{p3} = \sqrt{\frac{E_d}{\rho} \frac{(1 - \mu)}{(1 + \mu)(1 - 2\mu)}} \quad (4)$$

where V_{p1} and V_{p3} represent one and three-dimensional stress wave speeds, respectively; μ represents the Poisson's ration, and ρ is the density of materials.

Besides, these four groups of samples after curing for 28 d were also conducted for freeze-thaw tests using the rapid freezing method according to the Chinese standard JTS/T236-2019 [24]. The relative dynamic elastic modulus of P_n and P_{n2} is based on the transverse frequency and velocity of P-wave is obtained by the Eqs. (5) and (6), where f_0 is the initial transverse frequency, Hz; f_n is the transverse frequency after n-th cycles of freeze-thaw tests, Hz; V_{p10} is the initial one-dimensional velocity of P-wave, m/s; V_{p1n} is the one-dimensional velocity of P-wave after n-th cycles of freeze-thaw tests, m/s.

$$P_n = \frac{f_n^2}{f_0^2} \times 100\% \quad (5)$$

$$P_{n2} = \frac{V_{p1n}^2}{V_{p10}^2} \times 100\% \quad (6)$$

Different shapes and sizes of samples were prepared according to the mix proportions of L1 in Table 1 to determine the influence of size effect on the results of dynamic elastic modulus by the impact-echo method, thereby studying the feasibility of applying the impact-echo method to detect the frost resistance of practical structures. The sample sizes can be seen in Fig. 1.

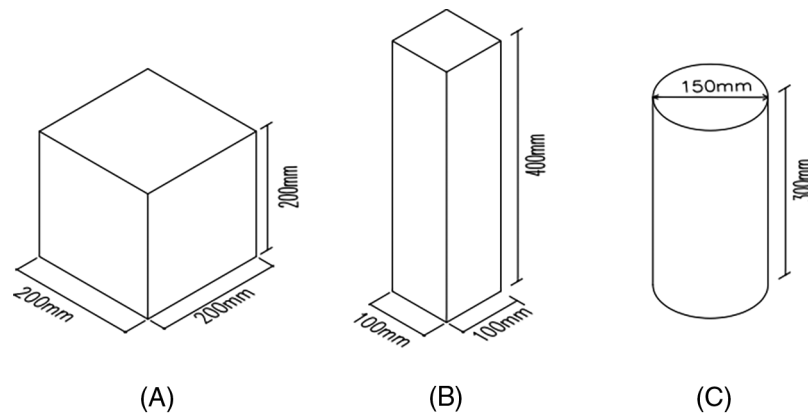


Figure 1: Designed size of samples for the size effect detecting

Samples with various section sizes of 100 mm × 100 mm × 400 mm, 150 mm × 150 mm × 400 mm, 200 mm × 200 mm × 400 mm, 250 mm × 250 mm × 400 mm, and 500 mm × 500 mm × 500 mm were prepared according to the mix proportions of L2 listed in Table 1 to investigate the change in frost resistance as a function of section sizes, so as to analysis the applicability of the impact-echo method in the detection of on-site concrete with different cross-sections. The velocity of P-wave was measured using the impact-echo method during the freeze-thaw process: where the layout of measuring points for the section size of 100 mm × 100 mm, 150 mm × 150 mm, 200 mm × 200 mm, 250 mm × 250 mm, and 500 mm × 500 mm are shown in Figs. 3a, 3b, 3d–3f, respectively.

2.3 Impact-Echo Measurement and Transverse Resonance Measurement

The DT-W18 dynamic elastic modulus tester produced by Beijing Shuzhi Yilong Instrument Co., Ltd. (China) was used to measure the transverse resonance frequency of the concrete. The frequency range of the device is 100–20 kHz, and the frequency sensitivity reaches 1 Hz.

The impact-echo method was conducted using a concrete structure multifunctional non-destructive tester (SCE-MATS, Sichuan Shengtuo Technology Co., Ltd., China) to test the P-wave velocity of concrete, and the dynamic elastic modulus of concrete was calculated inversely, as shown in Eq. (3). The equipment has a complete set of signal acquisition system and analysis system, which can perform MEM (maximum entropy method) analysis, FFT (fast Fourier transform) analysis, correlation analysis, waveform analysis, etc. Various defects in concrete structures such as the loss of strength and cracks can be detected.

The transverse frequency and P-wave velocity were measured by the transverse resonance method [11] and the impact-echo method [10], respectively. The schematic diagram of samples testing is shown in Fig. 2. The operation process of the transverse resonance method can be found in Chinese standard JTS304-2019. According to this standard, concrete specimens were placed on a polystyrene board with a thickness of 20 mm, and the forming surface of the specimen faced up on the board. The probe of the excitation transducer pressed lightly at 1/2 of the midline of the long side of the specimen. The probe of the receiver pressed lightly on the midline of the long side of the specimen and at a distance of 5 mm from the end face. The position of the measuring point was marked, and the length, width, and height (l, b, h) of the test block were measured prior to test, with a measurement accuracy of 1 mm. A layer of butter was coated on the contact surface between the probe and the specimen during the test as a coupling medium. The pressure value should be selected when absence of noise of the instrument was generated during the test. The frequency value was chosen the average of three measurements of specimens.

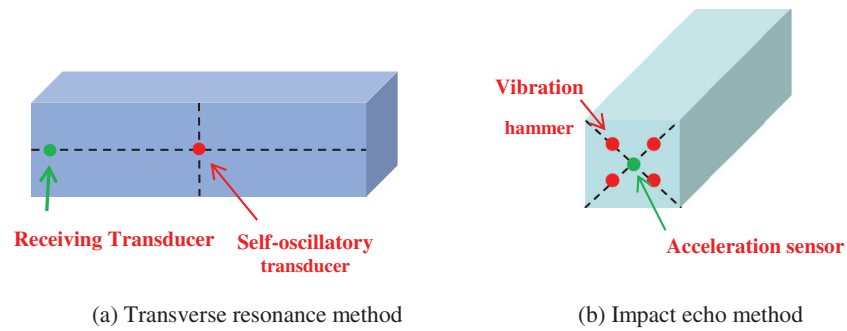


Figure 2: Schematic diagram of samples testing

For the impact-echo method [25], the measuring point arrangement is shown in Fig. 3. A stainless steel ball with a diameter of 17 mm is selected as the vibration hammer, the receiving point is located in the center of the end face, and four excitation points are arranged along the corner of the end face. Each measuring point is tested twice, and the average value of 8 readings (f , Hz) is taken as the test result. The test piece is placed on a polystyrene board with a thickness of 20 mm during the test.

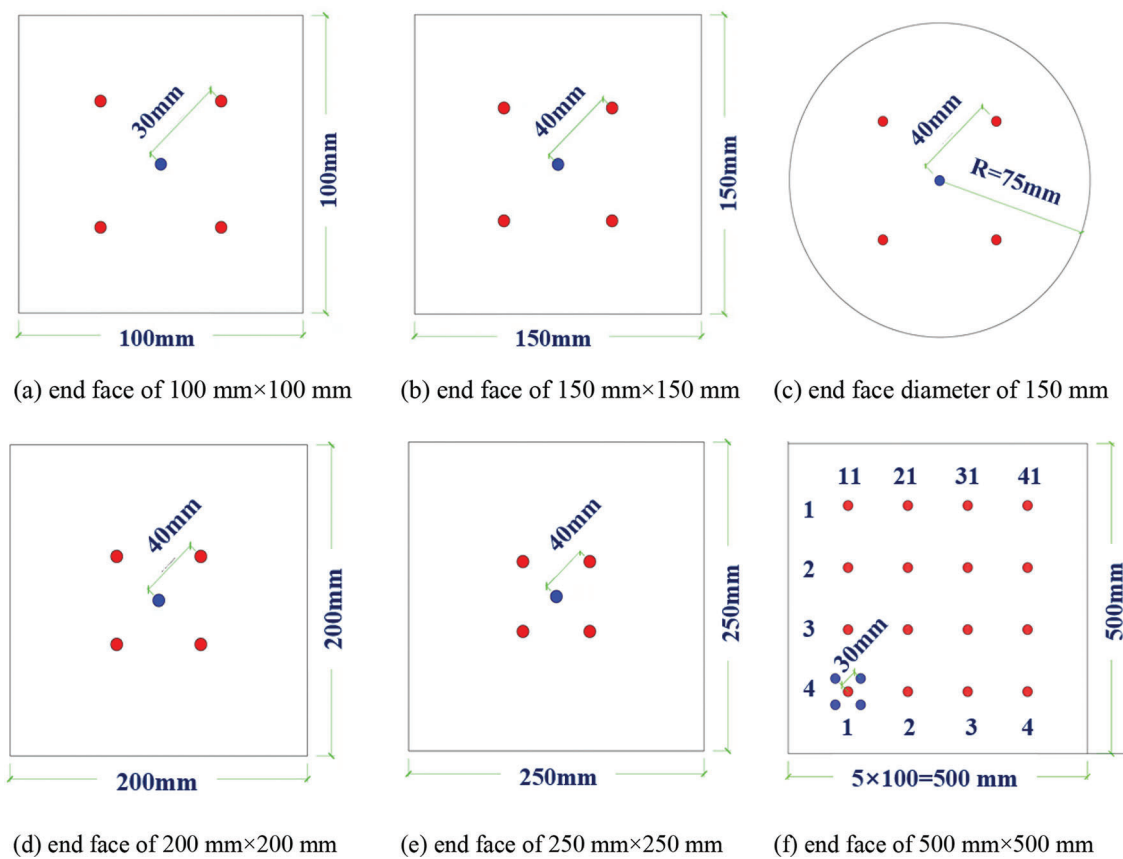


Figure 3: Layout of accelerometer (receiving point, the blue points) and impact points (the red points) for prism and cylinder specimens

3 Results and Discussion

3.1 Dynamic Modulus E_d

The comparison of dynamic elastic modulus obtained by impact-echo method and transverse resonance method is shown in Tables 2 and 3. Results show that the dynamic elastic modulus of concrete calculated from one-dimensional velocity of P-wave has little difference with that obtained by the transverse resonance method no matter the curing age of 7 or 28 d. The deviation ratio of these two methods decreased as the curing age prolonged, except for the S2 group. The deviation ratios of L2 group and S2 group at 7 d curing reached a higher level of 3.14% and 3.26%, respectively. All the deviation ratios of various groups decrease to less than 2% after 28 d of curing, which confirms that the impact-echo method calculated from velocity of P-wave can be used to detect the dynamic elastic modulus of concrete and has a high reliability. Previous research showed that the velocity of P-wave displays a high correlation with the curing age, curing conditions, the type and dosage of coarse aggregate, and is not sensitive to the type of cement, water-binder ratio, and sand coarse aggregate ratio [26]. The frequency caused by the instantaneous excitation of impact is low, and produces a relatively long wavelength. Almost no scattering caused by aggregates can be found because this wavelength is longer than the particle size of aggregates [27]. Therefore, the result obtained by the impact-echo method is independent of the majority external interference, increasing the accuracy of tests [28]. The spectrum diagram and time domain curve of S1–3 sample using impact-echo method are shown in Fig. 4.

Table 2: Results of dynamic elastic modulus of concrete after 7 d of curing obtained by impact-echo method and transverse resonance method

No.	Impact-echo method			Transverse resonance method			Δ_1 (%)	
	V_{p1} (m/s)	E_{d2} (GPa)	Avg. E_d (GPa)	f (Hz)	E_d (GPa)	Avg. E_d (GPa)		
L1	1	3997	38.53	38.50	2139	37.47	37.42	2.90
	2	3997	38.53		2130	37.18		
	3	3993	38.45		2143	37.61		
L2	1	3897	36.31	36.42	2079	35.10	35.31	3.14
	2	3906	36.48		2085	35.29		
	3	3906	36.48		2092	35.54		
S1	1	3989	37.90	37.91	2130	36.71	36.71	3.26
	2	3988	37.88		2131	36.74		
	3	3992	37.95		2130	36.69		
S2	1	3833	34.99	34.97	2057	34.23	34.40	1.67
	2	3831	34.95		2061	34.36		
	3	3832	34.97		2068	34.60		

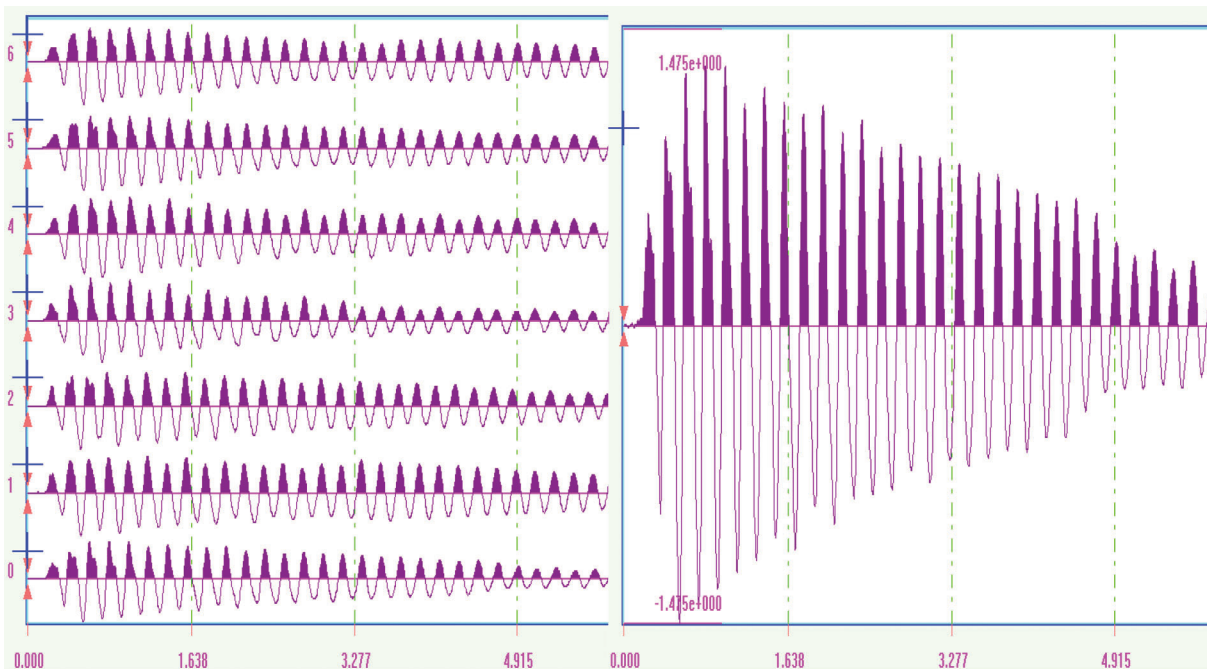
Note: Δ_1 : the deviation ratio of dynamic elastic modulus between the impact-echo method and transverse resonance method.

Table 3: Results of dynamic elastic modulus of concrete after 28 d of curing obtained by impact-echo method and transverse resonance method

No.	Impact-echo method			Transverse resonance method			Δ_2 (%)	
	V_{p1} (m/s)	E_{d2} (GPa)	Avg. E_d (GPa)	f (Hz)	E_d (GPa)	Avg. E_d (GPa)		
L1	1	4109	40.72	40.68	2213	40.12	40.13	1.37
	2	4111	40.76		2208	39.95		
	3	4101	40.56		2219	40.32		

(Continued)

Table 3 (continued)								
No.	Impact-echo method			Transverse resonance method			Δ_2 (%)	
	V_{pl} (m/s)	E_{d2} (GPa)	Avg. E_d (GPa)	f (Hz)	E_d (GPa)	Avg. E_d (GPa)		
L2	1	4015	38.54	38.95	2168	38.17	38.30	1.71
	2	4073	39.66		2174	38.38		
	3	4021	38.66		2173	38.35		
S1	1	4114	40.31	40.27	2220	39.88	39.89	0.95
	2	4110	40.23		2219	39.82		
	3	4112	40.27		2223	39.97		
S2	1	4018	38.46	38.39	2157	37.65	37.67	1.92
	2	4012	38.35		2157	37.64		
	3	4013	38.37		2160	37.73		



(a) spectrum diagram

(b) time domain curve

Figure 4: Spectrum diagram and time domain curve of S1–3 sample using impact-echo method

3.2 Frost-Resistance Property

Results of the mass loss and the value of P_n and P_{n2} of prismatic specimens after various cycles of freeze-thaw are shown in Tables 4–7. The P_n and P_{n2} are the relative dynamic elastic modulus (RDEM, %) based on the transverse frequency and velocity of P-wave, respectively, which can be calculated by Eqs. (5) and (6): The mass loss ratio (W_1 , %) can be calculated by Eq. (7): where W_0 is the initial mass of samples; W_n is the mass of sample after n-th cycles of freeze-thaw tests. Tables 4–7 show that the

greatest mass loss of 1.07% was found after 50-th freeze-thaw cycles of S1. A low deformation of the longitudinal and transverse on samples was found during the freeze-thaw tests, so the size, Poisson ratio, and density of samples are considered as almost unchanged during tests.

$$W_1 = \frac{W_n - W_0}{W_0} \times 100\% \quad (7)$$

Table 4: Frost-resistance test results for L1 specimens based on resonance frequency and elastic wave velocity

Cycle of freeze-thaw test	f (Hz)	P_n (%)	V_{pl} (m/s)	P_{n2} (%)	$P_n - P_{n2}$ (%)	Mass loss ratio, W_1 (%)
0	2213	100.00	4107	100.00	0	0
25	2163	95.53	4023	95.95	-0.42	0.84
50	2088	89.02	3937	91.89	-2.87	1.01
75	1805	66.53	3376	67.57	-1.04	0.91
100	1076	23.64	2109	26.37	-2.73	0.99

Table 5: Frost-resistance test results for L2 specimens based on resonance frequency and elastic wave velocity

Cycle of freeze-thaw test	f (Hz)	P_n (%)	V_{pl} (m/s)	P_{n2} (%)	$P_n - P_{n2}$ (%)	Mass loss ratio, W_1 (%)
0	2172	100.00	4036	100.00	0	0
25	1950	80.60	3720	84.95	-4.35	0.69
50	1337	37.89	2651	43.14	-5.25	0.86

Table 6: Frost-resistance test results for S1 specimens based on resonance frequency and elastic wave velocity

Cycle of freeze-thaw test	f (Hz)	P_n (%)	V_{pl} (m/s)	P_{n2} (%)	$P_n - P_{n2}$ (%)	Mass loss ratio, W_1 (%)
0	2221	100.00	4112	100.00	0	0
25	2154	94.06	4019	95.53	-1.47	0.87
50	2026	83.21	3790	84.95	-1.74	1.07
75	1764	63.08	3464	70.97	-7.89	0.87
100	1046	22.18	2062	25.15	-2.97	0.96

Table 7: Frost-resistance test results for S2 specimens based on resonance frequency and elastic wave velocity

Cycle of freeze-thaw test	f (Hz)	P_n (%)	V_{pl} (m/s)	P_{n2} (%)	$P_n - P_{n2}$ (%)	Mass loss ratio, W_1 (%)
0	2158	100.00	4014	100.00	0.00	0
25	1869	75.01	3550	78.22	-3.21	0.12
50	1253	33.71	2451	37.28	-3.57	0.83

Results of regression analysis based on the least square method between E_d and V_{p1} , V_{p1} and f of four groups of prismatic specimens are presented in Table 8, which substantially conforms the relation of $V_{p1} = 1.843f$. E_d is proportional to the square of V_{p1} , and all of regression analyses have a high correlation coefficient of larger than 0.99.

Table 8: Regression equation of impact-echo method

L1	$V_{p1} = 1.7781f + 0.1988$ $R^2 = 0.9992$	$E_d = 1.8764 \times 10^{-5} V_{p1}^{2.1578}$ $R^2 = 0.9995$
L2	$V_{p1} = 1.6769f + 0.4176$ $R^2 = 0.9984$	$E_d = 1.5501 \times 10^{-5} V_{p1}^{2.2873}$ $R^2 = 0.9988$
S1	$V_{p1} = 1.7437f + 0.2771$ $R^2 = 0.9943$	$E_d = 1.7637 \times 10^{-5} V_{p1}^{2.2218}$ $R^2 = 0.9988$
S2	$V_{p1} = 1.7360f + 0.2829$ $R^2 = 0.9994$	$E_d = 1.7249 \times 10^{-5} V_{p1}^{2.2137}$ $R^2 = 0.9998$

Results of P_{n2} of the four groups of samples show a well correlation with that of P_n , as shown in Figs. 5 and 6. All the deviation ratios between the P_{n2} and P_n are less than 5%, except for the S2 group (reaching 7.89% at 75-th cycles). In all groups, the P_{n2} is slightly larger than P_n , indicating that the relative dynamic elastic modulus calculated by velocity of P-wave is larger than that calculated by the transverse frequency. Therefore, real-time detection of the velocity of P-wave of concrete can be used to monitor the change of relative dynamic elastic modulus of the actual structure [29–32], so as to analyze the degradation degree of concrete during freeze-thaw cycles.

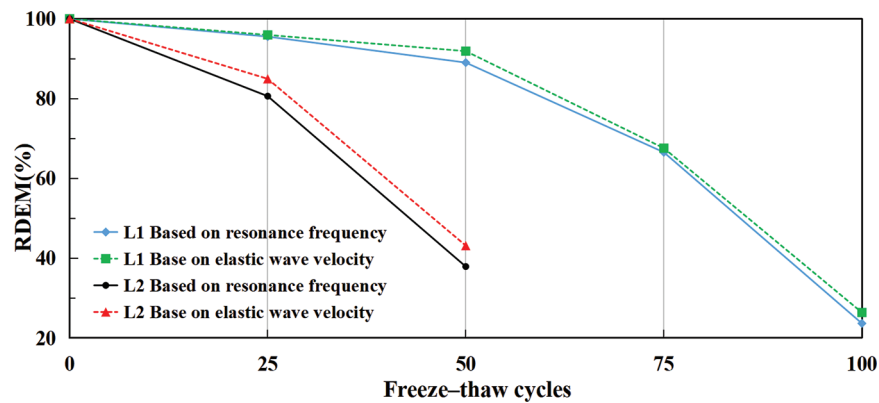


Figure 5: Curves of relative dynamic elastic modulus (REDM) changed with freeze-thaw cycles for L1 and L2 specimens

The frost-resistance properties of L1 group is better than that of L2 group; Similarly, the frost-resistance properties of S1 group is better than that of S2 group, which reveals that using a smaller water-cement ratio is beneficial to improve the frost resistance of concrete. Lu et al. [33] also found that the lower the water-cement ratio, the stronger the ability to resist freeze-thaw cycles of ultra-high performance concrete. Freeze-thaw cycle tests were conducted by Zhao et al. [34] on concrete with different maximum particle sizes of coarse aggregates (9.5, 19, 26.5, 31.5, and 37.5 mm), and found that the relative dynamic elastic modulus decreased with the increase of the maximum particle size of coarse aggregates. The frost heave appeared on the coarse aggregate when the particle size exceeded 31.5 mm. Dalibor et al. [35] found that the relative dynamic elastic modulus decreased rapidly after the 50 cycles of freeze-thaw tests when the maximum particle size of coarse aggregates was within 16 mm ($w/c \geq 0.5$), which is very similar to the test results of sample S2 in Fig. 6.

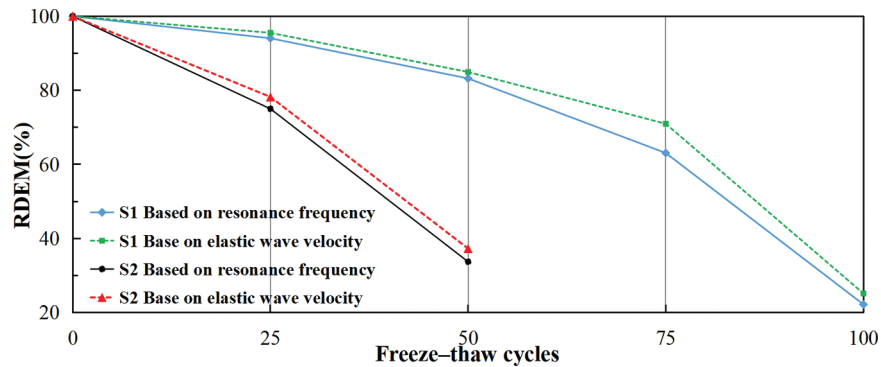


Figure 6: Curves of relative dynamic elastic modulus (REDM) changed with freeze-thaw cycles for S1 and S2 specimens

Both relative dynamic elastic modulus displayed a relatively mild decrease before 50-th cycles and showed a sharp decrease afterwards. The decrease in relative dynamic elastic modulus indicates that the damage has been appeared in internal structure, thereby reducing the compaction as well. The damage is accelerated in a relatively loose structure during the subsequent freeze-thaw cycles, extending the propagation time of elastic waves in concrete, which results in a sharper decrease in relative dynamic elastic modulus. For example, when the $P_n < 60\%$ (freeze-thaw cycles is ranging from 75-th to 100-th for L1 and S1 groups, and 25-th to 50-th for L2 and S2 groups), the V_{p1} of L1 group decreased from 3376 to 2109 m/s, with a V_{p3} decreasing from 3558 to 2223 m/s. Similarly, V_{p3} of L1, L2, S1, and S2 groups decreased by 37.5%, 28.3%, 40.5%, and 40.0%, respectively. At this conditions, the value of V_{p3} is lower than 3600 m/s, the general standard of concrete quality evaluation [36], indicating a serious internal damage of concrete caused by freeze-thaw cycles.

3.3 Size Effect of Impact-Echo Method

The port hydraulic structure has characteristics of various cross-section and a relatively large volume in actual engineering. For example, the front structure of the gravity wharf (breast wall, caisson, buttress, etc.) has various forms, and the cross-section has rectangular, circular, stepped, etc. [37,38]; In-service concrete structures need to be evaluated by inspection of their different structural elements to determine their durability [39–43]. Methodologies have been developed in different countries to estimate the health of structure through inspection [44–58].

The reinforced concrete structure is usually used to improve its strength, rigidity, and integrity. Therefore, various shapes and sizes of samples were designed to explore the size effect on the velocity of elastic wave, and the results can be found in Table 9. It indicates that the shape and size have scarcely influence on the velocity of elastic wave at a specific curing age, indicating that this method is suitable for the detecting of a physical engineering. The maximum deviation is just 2.1%, occurring between the cube samples and cuboid sample at 7 d of curing. The velocity of elastic wave shows an obvious increase during the early age and becomes level off afterwards. This trend is consistent with that of strength development due to the forming of a compacter microstructure of concrete as a function of the curing age.

3.4 Frost-Resistance Property of Various Cross-Section Size Samples Detected by Impact-Echo Method

Based on the results of the fact that the velocity of P-wave is independent of the shape and size of samples, the frost-resistance property of samples with various cross-section size was investigated and results are listed in Table 10. The decrease trends of velocity of P-wave and relative dynamic elastic modulus for the cross-section size of 100 and 150 mm is generally the same after 75-th freeze-thaw

cycles, decreasing to 36.10% and 36.93% of the initial value, respectively. In comparison, the relative dynamic elastic modulus for the cross-section size of 200 and 250 mm decreases only to 78.40% and 80.66% of the initial value, respectively, indicating that the damage of larger cross-section size groups is far less than that of the smaller groups.

Table 9: Results of elastic wave velocity of concrete as a function of curing age and size effect

Samples		Elastic wave velocity (m/s)			
Shape	Size (mm)	3 d	7 d	14 d	28 d
Cube	200 × 200 × 200	3634	3817	3986	4027
Cuboid	100 × 100 × 400	3663	3897	3979	4006
Cylinder	φ150 × 300	3656	3861	3950	4014

Table 10: Frost-resistance results of prismatic concrete specimens as a function of cross-section size

Size (mm)	Freeze–thaw cycles	V_p (m/s)	P_n (%)	Size (mm)	freeze–thaw cycles	V_p (m/s)	P_n (%)
100 × 100 × 400	0	4036	100.00	150 × 150 × 400	0	3987	100.00
	25	3720	84.95		25	3642	83.44
	50	2651	43.14		50	2798	49.25
	75	2425	36.10		75	2423	36.93
200 × 200 × 400	0	3928	100.00	250 × 250 × 400	0	3916	100.00
	25	3823	94.73		25	3817	95.00
	50	3719	89.64		50	3714	89.95
	75	3478	78.40		75	3517	80.66

In addition, a larger volume sample with a dimension of 500 mm × 500 mm × 500 mm was prepared to further explore changes in the degree of freeze-thaw damage as a function of the section thickness. The schematic diagram of samples testing and measuring-point arrangement are shown in Figs. 7 and 3f, respectively, and results are shown in Fig. 8. Results show that the degree of damage can be obviously divided into three regions. For example, the relative dynamic elastic modulus can be divided into three ranges of 75%–80%, 85%–90%, and 90%–95% after 100-th freeze-thaw cycles, and the RDEM distribution diagram can be found in Fig. 9. It can be seen that the 75%–80% region is located at the four corners of the specimen, 85%–90% region is located at the remaining edges of the specimen, and 90%–95% region is located at the center of the specimen. The degree of erosion damage of the center of specimen is much slighter than that of the external rim regions.

It spends a longer period for the center of the cross-section to drop a same temperature as the cross-section size of samples increased, because the specific heat capacity of concrete remains unchanged during the processes of freeze-thaw cycles. This indicates that the decrease in the relative dynamic elastic modulus reduced from the surface to the inner layer; that is, the surface is expected to be the most vulnerable part for the freeze-thaw damage. The outside of concrete protects the inter part from the freeze-thaw damage; so if the size of the specimen is large enough, the internal concrete is likely not to be damaged during freeze-thaw cycles, just like the flowing water under the ice in winter.



Figure 7: Schematic diagram of samples testing (500 mm × 500 mm × 500 mm) using impact-echo method

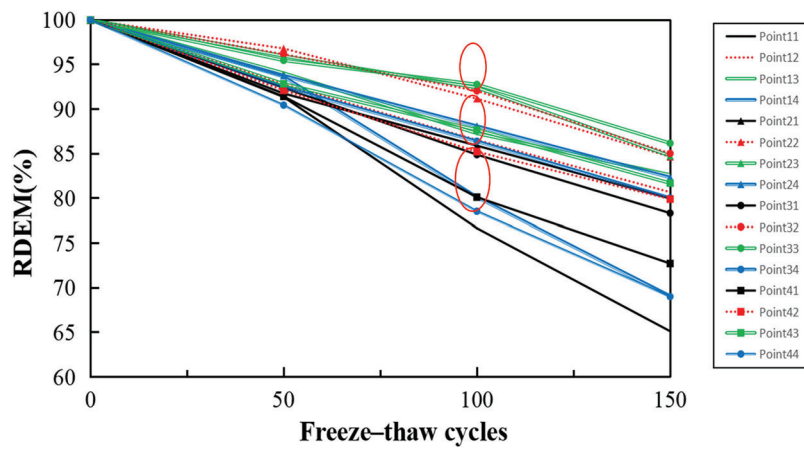


Figure 8: RDEM obtained from different measuring points of prismatic concrete (500 mm × 500 mm × 500 mm) as a function of freeze-thaw cycles

Point 11 76.67%	Point 12 86.52%	Point 13 87.27%	Point 14 80.13%
Point 21 85.90%	Point 22 91.17%	Point 23 92.41%	Point 24 88.10%
Point 31 84.89%	Point 32 92.05%	Point 33 92.76%	Point 34 86.39%
Point 41 80.12%	Point 42 85.22%	Point 43 87.66%	Point 44 78.54%

Figure 9: RDEM distribution diagram of a 500 mm × 500 mm × 500 mm specimen with 100-th freeze-thaw cycles

3.5 Applicability Analysis of Impact-Echo Method for the Detecting of Frost-Resistance Property for On-Site Structures

In fact, the major freeze-thaw damage usually displays on the surface of hydraulic structure. The damage of accompanying samples conducted by the laboratory freeze-thaw cycles is much more serious than that of the practical structure. For example, many core samples have been damaged but the practical structure only showed honeycomb or pockmark. The laboratory samples have been subjected to 200 freeze-thaw cycles, but the practical structure on site may have only subjected to 125 times. Therefore, the laboratory freeze-thaw testing cannot reflect the damage of practical structure very well. The impact-echo method is suitable for on-site non-destructive testing of practical structure, and is expected to have a more widely application in detecting the frost-resistance property.

The velocity of P-wave of concrete is not greatly affected by the size effect. The impact-echo method has good accuracy and strong practicability, and can be used to evaluate the frost-resistance property of large-volume hydraulic concrete structures on site. A high-frequency monitoring is needed for the detecting of structural deformation, displacement, temperature, stress, or other parameters. However, a high-frequency monitoring is unnecessary when using the impact-echo method due to the relatively slow progress of concrete durability deterioration. The impact-echo method can be used to test the P-wave velocity of concrete every year or several years according to the importance of the structure and the degree of damage. The speed and trend for durability degradation of concrete can be fully obtained through the accumulation, analysis, and prediction of test data. This is of great significance to the detecting for frost-resistance property of large-volume hydraulic concrete.

Currently, according to the Chinese standard JTS304-2019, the detection method of freeze-resistance properties for on-site hydraulic concrete is that: After drilling the core sample on the surface of the concrete structure, the core sample is sawed and cut into two pieces, one of which has a surface affected by freezing and thawing, and the other is not affected by freezing and thawing. The rapid freeze and thaw cycle tests were carried out on these two core samples. The current freeze-thaw damage of the original structure and the remaining service life are estimated by comparison the two core samples. The disadvantage of this method is that it requires a “quick freezing” test, which is cumbersome and time-consuming. The frost resistance property of structure can be directly evaluated when using the impact-echo technology. The P-wave velocity of the two core samples is needed to be measured for the calculation of the relative dynamic elastic modulus. P-wave velocity tests are needed only on the surface of the structure when the structure is tested for durability again, which avoids coring again. One cycle of freeze-thaw test lasted 13–14 h and 2.5–3 h, respectively. After 100 cycles of freeze-thaw, the relative dynamic elastic moduli dropped to 10% and 90%, respectively, indicating that the large specimens have a better frost resistance property. The results of in-situ tests of the loss in relative dynamic elastic moduli during frost resistance tests of large-size structure is cannot be replaced by laboratory tests conducted on core samples. Therefore, the impact-echo technology cannot be replaced by the traditional resonance frequency method in detecting the frost resistance property of large-size concrete structures on-site.

Based on the above experimental results, the frost resistance of the structure in the actual project (the 300,000-ton crude oil terminal project in the Rongxing Port Area of Panjin Port) have been evaluated by using the impact-echo method. The thickness of a pier is 3 m with a design strength of 45 MPa, and a design level of freeze thaw durability of F350. The results show that the impact-echo method has a higher accuracy in evaluating the frost resistance of large-size hydraulic concrete compared to the ultrasonic method and resonance method. The impact-echo method has a high reliability proved by repeatability tests and reproducibility tests. It proves that the impact-echo technology has good applicability for on-site testing of the durability of concrete structures in water transportation projects.

4 Conclusions

The feasibility of the impact-echo method to obtain the relative dynamic elastic modulus is explored to detect the frost-resistance property of large-volume hydraulic concrete on site. A comparison between the impact-echo method and the traditional resonance frequency method in detecting the relative dynamic elastic modulus is also conducted. We make the following conclusions:

The impact-echo method can replace the traditional resonance frequency method to evaluate the frost resistance of concrete, and has advantages of high accuracy, easy to operate, and not limiting to the size of aggregates and samples. Thus, the impact-echo method can be used to evaluate the frost-resistance property of large-volume hydraulic structure on site by detecting the relative dynamic elastic modulus without drilling core, which is more convenient to operate than traditional resonance method. The dynamic elastic modulus of concrete detected by the impact-echo method has little difference with that obtained by the transverse resonance method. The deviation between the two methods is controlled within 2% for the dynamic modulus of elasticity, and within 5% for the relative dynamic elastic modulus of elasticity. The one-dimensional P-wave velocity of concrete has a good linear correlation with the transverse resonance frequency, which substantially conforms the $V_{pl} = 1.843f \cdot E_d$ is proportional to the square of V_{pl} , and all of regression analyses have a high correlation coefficient of larger than 0.99.

The velocity of P-wave of concrete is not greatly affected by the size effect, while the frost resistance of concrete is greatly affected by the size effect. A reduction of the water-cement ratio is beneficial to improve the frost resistance of concrete. The freeze-thaw damage develops from the surface to the inner layer, and the surface is expected to be the most vulnerable part for the freeze-thaw damage. For example, the relative dynamic elastic modulus decreases to 36% of the initial value when the side length of samples is not greater than 150 mm. For the large-size concrete specimens, the relative dynamic elastic modulus of samples with side lengths of 200 and 250 mm are 78% and 81% of the initial value. The relative dynamic elastic modulus of the edge position of concrete is 13% lower than that in the central position. It is expected to monitor and track the degradation of the frost resistance of the actual structure by frequently detecting the P-wave velocity on site.

Funding Statement: This work was financed by Hainan Provincial Natural Science Foundation of China (522QN279) and the Research Lab Construction of Hainan University (ZY2019HN0904).

Conflicts of Interest: The authors declare that they have no conflicts of interest to report regarding the present study.

References

1. Mehta, P. K. (1991). Durability of concrete-fifty years of progress. *Proceedings of the 2nd International Conference on Durability of Concrete*, Detroit, USA.
2. Zhao, X., Lv, X., Wang, L., Zhu, Y., Dong, H. et al. (2015). Research of concrete residual strains monitoring based on WLI and FBG following exposure to freeze-thaw tests. *Cold Regions Science and Technology*, 116, 40–48. <https://doi.org/10.1016/j.coldregions.2015.04.007>
3. Wu, Y., Hubbard, S. S., Ulrich, C., Wulschleger, S. D. (2013). Remote monitoring of freeze-thaw transitions in Arctic soils using the complex resistivity method. *Vadose Zone Journal*, 12(1), 1–13. <https://doi.org/10.2136/vzj2011.0176>
4. Arnfelt, H. (1943). Damage on concrete pavements by winter time salt treatment. Statens Vaeginst (Sweden).
5. Skripkiūnas, G., Nagrockienė, D., Girskas, G., Vaičienė, M., Baranauskaitė, E. (2013). The cement type effect on freeze-thaw and deicing salt resistance of concrete. *Procedia Engineering*, 57, 1045–1051. <https://doi.org/10.1016/j.proeng.2013.04.132>

6. Wang, L., Cao, Y., Wang, Z., Du, P. (2013). Evolution and characterization of damage of concrete under freeze-thaw cycles. *Journal of Wuhan University of Technology-Materials Science Edition*, 28(4), 710–714. <https://doi.org/10.1007/s11595-013-0757-7>
7. Cao, J. G., Li, J. Y., Lin, L., Tian, J. T., Guan, Y. S. et al. (1999). Study on frost-resistance of high-strength concrete. *Journal of Building Materials*, 2(4), 292–297.
8. Powers, T. C. (1938). Measuring young's modulus of elasticity by means of sonic vibrations. *Proceedings of American Society of Testing Materials*, 38, 460–469.
9. Su, H., Lin, W. Z. (2003). Impact-echo method and ITS application to civil engineering. *Nondestructive Testing*, 26(3), 81–83 (in Chinese).
10. ASTM C1383 (2000). Test method for measuring the P-wave speed and the thickness of concrete plates using the impact-echo method. USA: American Society of Testing Materials.
11. ASTM C125 (2008). Standard test method for fundamental transverse, longitudinal, and torsional resonant frequencies of concrete specimens. USA.
12. Liang, M. T., Su, P. J. (2001). Detection of the corrosion damage of rebar in concrete using impact-echo method. *Cement and Concrete Research*, 31, 1427–1436. [https://doi.org/10.1016/S0008-8846\(01\)00569-5](https://doi.org/10.1016/S0008-8846(01)00569-5)
13. Krzemień, K., Hager, I. (2015). Post-fire assessment of mechanical properties of concrete with the use of the impact-echo method. *Construction and Building Materials*, 96, 155–163. <https://doi.org/10.1016/j.conbuildmat.2015.08.007>
14. Azari, H., Nazarian, S., Yuan, D. (2014). Assessing sensitivity of impact echo and ultrasonic surface waves methods for nondestructive evaluation of concrete structures. *Construction and Building Materials*, 71, 384–391. <https://doi.org/10.1016/j.conbuildmat.2014.08.056>
15. Chaudhary, M. T. A. (2013). Effectiveness of impact echo testing in detecting flaws in prestressed concrete slabs. *Construction and Building Materials*, 47, 753–759. <https://doi.org/10.1016/j.conbuildmat.2013.05.021>
16. Hsu, K. T., Cheng, C. C., Lin, Y. (2008). Use impact-echo method to evaluate bond of reinforced concrete subjected to early-age vibration. *Journal of Solid Mechanics and Materials Engineering*, 2(12), 1528–1538. <https://doi.org/10.1299/jmmp.2.1528>
17. Zima, B. (2019). Guided wave propagation in detection of partial circumferential debonding in concrete structures. *Sensors*, 19, 1–19. <https://doi.org/10.3390/s19092199>
18. Wandowski, T., Kudela, P., Ostachowicz, W. M. (2019). Numerical analysis of elastic wave mode conversion on discontinuities. *Composite Structures*, 215, 317–330. <https://doi.org/10.1016/j.compstruct.2019.02.076>
19. Jaganathan, A. P. (2019). Multichannel surface wave analysis of reinforced concrete pipe segments using longitudinal and circumferential waves induced by a point impact. *Journal of Applied Geophysics*, 163, 40–54. <https://doi.org/10.1016/j.jappgeo.2019.02.010>
20. Hamid, G. A. (2008). Long-term bridge performance program. *Fourth US-Taiwan Bridge Engineering Workshop*.
21. Wang, W., Lu, C., Yuan, G., Zhang, Y. (2017). Effects of pore water saturation on the mechanical properties of fly ash concrete. *Construction and Building Materials*, 130, 54–63. <https://doi.org/10.1016/j.conbuildmat.2016.11.031>
22. Dvoák, R., Topolá, L. (2021). Effect of hammer type on generated mechanical signals in impact-echo testing. *Materials*, 14, 606–624. <https://doi.org/10.3390/ma14030606>
23. SL352-2020 (2021). *Test code for hydraulic concrete*. Beijing, China: China Water & Power Press.
24. JTS/T 236-2019 (2019). *Technical specification for concrete testing of port waterway engineering*. Beijing, China: China Communications Press Co., Ltd.
25. Lu, X., Sun, Q., Feng, W., Tian, J. (2013). Evaluation of dynamic modulus of elasticity of concrete using impact-echo method. *Construction and Building Materials*, 47, 231–239. <https://doi.org/10.1016/j.conbuildmat.2013.04.043>
26. Kee, S. H., Lee, J. W., Candelaria, M. D. (2020). Evaluation of delamination in concrete by ie testing using multi-channel elastic wave data. *Sensors*, 20, 201–220.

27. Wu, X., Yan, Q., Hedayat, A., Wang, X. (2021). The influence law of concrete aggregate particle size on acoustic emission wave attenuation. *Scientific Reports*, 11(1), 1–14. <https://doi.org/10.1038/s41598-021-02234-x>
28. Lu, X., Ma, F., Luke, A., Wang, R. (2015). Assessing frost resistance of concrete by impact-echo method. *Magazine of Concrete Research*, 67, 317–324. <https://doi.org/10.1680/mac.14.00051>
29. Lin, J., Sansalone, M. (1997). A procedure for determining P-wave speed in concrete for use in impact echo testing using a Rayleigh wave speed measurement technique. *Innovations in Nondestructive Testing of Concrete*, 168, 137–166.
30. Sansalone, M., Carino, N. J. (1986). *Impact-echo: A method for flaw detection in concrete using transient stress waves*. National Bureau of Standards.
31. Cheng, C., Sansalone, M. (1995). Determining the minimum crack width that can be detected using the impact-echo method Part 1: Experimental study. *Materials and Structures*, 28, 74–82. <https://doi.org/10.1007/BF02473174>
32. Hsiao, C., Cheng, C. C., Liou, T., Juang, Y. (2008). Detecting flaws in concrete blocks using the impact-echo method. *NDT & E International*, 41, 98–107.
33. Lu, Z., Feng, Z., Yao, D., Li, X., Ji, H. (2021). Freeze-thaw resistance of ultra-high performance concrete: Dependence on concrete composition. *Construction and Building Materials*, 293, 123523–123532. <https://doi.org/10.1016/j.conbuildmat.2021.123523>
34. Zhao, S., Xia, J. (2011). Durability based indexes of coarse aggregate for cement concrete. *Advanced Materials Research*, 31, 1941–1946. <https://doi.org/10.4028/www.scientific.net/AMR.250-253.1941>
35. Dalibor, K., Tomáš, V., Barbara, K. (2018). Influence of coarse aggregate grain size on frost resistance of concrete. *Rehabilitation and Reconstruction of Buildings*, 776, 37–40.
36. Leslie, J. R., Cheeseman, W. J. (1949). An ultrasonic method for studying deterioration and creaking in concrete structures. *American Concrete Institute Proceedings*, 46, 17–36.
37. Pirooznia, A., Moradloo, A. J. (2020). Investigation of size effect and smeared crack models in ordinary and dam concrete fracture tests. *Engineering Fracture Mechanics*, 226(1), 106863–106887. <https://doi.org/10.1016/j.engfracmech.2019.106863>
38. Huang, Y., Xiao, L., Gao, J., Liu, Y. (2019). Tensile creep and unloading creep recovery testing of dam concrete with fly ash. *Journal of Materials in Civil Engineering*, 31(5), 05019001.1–05019001.7. [https://doi.org/10.1061/\(ASCE\)MT.1943-5533.0002682](https://doi.org/10.1061/(ASCE)MT.1943-5533.0002682)
39. Xiao, M., Zhang, S., Tang, Y., Lin, Z., Chen, J. (2016). A study of a real-time online monitoring system for the durability of concrete structures. *Anti-Corrosion Methods & Materials*, 63(3), 184–189. <https://doi.org/10.1108/ACMM-11-2015-1608>
40. Fang, X., Yin, Z., Chen, H., Ni, J., Zhang, D. et al. (2021). Comparison study on durability monitoring and inspection for reinforced concrete structure in marine environment. *The Ocean Engineering*, 39(6), 111–118.
41. Yang, H., Hu, Z., Yu, F., Fang, Z. (2019). Field test and evaluation analysis on durability of fly ash concrete structures in seawater environment. *The Ocean Engineering*, 37(2), 104–111.
42. Chaleel, W., Cheewaket, T., Jaturapitakkul, C. (2021). Utilization of recycled aggregate concrete for marine site based on 7-year field monitoring. *International Journal of Concrete Structures and Materials*, 15, 34–44. <https://doi.org/10.1186/s40069-021-00473-w>
43. Torres-Acosta, A. A., Patron-Solares, A., Alcantara-Lagunes, P. (2020). Durability health monitoring during construction of concrete structures in marine environment. *Structural Control and Health Monitoring*, 28(3), e2674–e2675.
44. Madani, H. M., Dolatshahi, K. M. (2020). Strength and stiffness estimation of damaged reinforced concrete shear walls using crack patterns. *Structural Control and Health Monitoring*, 7(4), e2494.1–e.2494.18. <https://doi.org/10.1002/stc.2494>
45. Raja, B. N. K., Miramini, S., Duffield, C., Sofi, M., Mendis, P. et al. (2020). The influence of ambient environmental conditions in detecting bridge concrete deck delamination using infrared thermography (IRT). *Structural Control and Health Monitoring*, 27(4), e2506–e2521. <https://doi.org/10.1002/stc.2506>

46. An, Y., Chatzi, E., Sim, S. H., Laflamme, S., Blachowski, B. (2019). Recent progress and future trends on damage identification methods for bridge structures. *Structural Control and Health Monitoring*, 26(10), e2416–e2445. <https://doi.org/10.1002/stc.2416>
47. Yang, C., Li, L., Li, J. (2020). Service life of reinforced concrete seawalls suffering from chloride attack: Theoretical modelling and analysis. *Construction and Building Materials*, 263(4), 120172–120185. <https://doi.org/10.1016/j.conbuildmat.2020.120172>
48. Jin, M., Ma, Y., Zeng, H., Liu, J., Gu, Y. (2020). Developing a multi-element sensor to non-destructively monitor several fundamental parameters related to concrete durability. *Sensors*, 20(19), 5607–5634. <https://doi.org/10.3390/s20195607>
49. Wei, B., Liu, B., Yuan, D., Mao, Y., Yao, S. (2021). Spatiotemporal hybrid model for concrete arch dam deformation monitoring considering chaotic effect of residual series. *Engineering Structures*, 228(1), 111488–111501. <https://doi.org/10.1016/j.engstruct.2020.111488>
50. Zima, B., Kdra, R. (2020). Baseline-free debonding detection in reinforced concrete structures by elastic wave propagation. *Measurement*, 172, 108907–108921. <https://doi.org/10.1016/j.measurement.2020.108907>
51. Li, D., Yang, K., He, Z., Zhou, H., Li, J. (2020). Acoustic emission wave velocity attenuation of concrete and its application in crack localization. *Sustainability*, 12(8), 7405–7418. <https://doi.org/10.3390/su12187405>
52. Liu, Z., Ma, C., Wei, X. (2021). P-wave velocity and energy evolution process of concrete in uniaxial loading-unloading tests. *Journal of Materials in Civil Engineering*, 33(6), 04021110.1–04021110.10. [https://doi.org/10.1061/\(ASCE\)MT.1943-5533.0003723](https://doi.org/10.1061/(ASCE)MT.1943-5533.0003723)
53. Kang, F., Li, J., Zhao, S., Wang, Y. (2019). Structural health monitoring of concrete dams using long-term air temperature for thermal effect simulation. *Engineering Structures*, 180(2), 642–653. <https://doi.org/10.1016/j.engstruct.2018.11.065>
54. Basu, S., Thirumalaiselvi, A., Sasmal, S., Kundu, T. (2021). Nonlinear ultrasonics-based technique for monitoring damage progression in reinforced concrete structures. *Ultrasonics*, 115, 106472–106484. <https://doi.org/10.1016/j.ultras.2021.106472>
55. Wang, Z., Markham, A. (2020). Wirelessly powered embedded sensor nodes for internal structural health monitoring. *IEEE Transactions on Industrial Electronics*, (99), 3013536–3013544.
56. Heitner, B., O'Brien, E. J., Yalamas, T., Schoefs, F., Leahy, C. et al. (2019). Updating probabilities of bridge reinforcement corrosion using health monitoring data. *Engineering Structures*, 190(7), 41–51. <https://doi.org/10.1016/j.engstruct.2019.03.103>
57. Kang, F., Li, J., Dai, J. (2019). Prediction of long-term temperature effect in structural health monitoring of concrete dams using support vector machines with Jaya optimizer and salp swarm algorithms. *Advances in Engineering Software*, 131, 60–76. <https://doi.org/10.1016/j.advengsoft.2019.03.003>
58. Wang, C., Xiao, J., Zhang, C., Xiao, X. (2020). Structural health monitoring and performance analysis of a 12-story recycled aggregate concrete structure. *Engineering Structures*, 205, 110102.1–110102.18. <https://doi.org/10.1016/j.engstruct.2019.110102>